Intense paramagnon excitations in a large family of high-temperature superconductors

M. Le Tacon[1]*, G. Ghiringhelli[2], J. Chaloupka[1], M. Moretti Sala[2], V. Hinkov[1,3], M. W. Haverkort[1], M. Minola[2], M. Bakr[1], K. J. Zhou[4], S. Blanco-Canosa[1], C. Monney[4], Y. T. Song[1], G. L. Sun[1], C. T. Lin[1], G. M. De Luca[5], M. Salluzzo[5], G. Khaliullin[1], T. Schmitt[4], L. Braicovich[2] and B. Keimer[1]*

In the search for the mechanism of high-temperature superconductivity, intense research has been focused on the evolution of the spin excitation spectrum on doping from the antiferromagnetic insulating to the superconducting state of the cuprates. Because of technical limitations, the experimental investigation of doped cuprates has been largely focused on low-energy excitations in a small range of momentum space. Here we use resonant inelastic X-ray scattering to show that a large family of superconductors, encompassing underdoped $YBa_2Cu_4O_8$ and overdoped $YBa_2Cu_3O_7$, exhibits damped spin excitations (paramagnons) with dispersions and spectral weights closely similar to those of magnons in undoped cuprates. The comprehensive experimental description of this surprisingly simple spectrum enables quantitative tests of magnetic Cooper pairing models. A numerical solution of the Eliashberg equations for the magnetic spectrum of $YBa_2Cu_3O_7$ reproduces its superconducting transition temperature within a factor of two, a level of agreement comparable to that of Eliashberg theories of conventional superconductors.

The 25th anniversary of the discovery of high-temperature superconductivity is approaching without a clear and compelling theory of the mechanism underlying this phenomenon. After the discovery of an unconventional (d-wave) symmetry of the Cooper-pair wavefunction in the copper oxides, the thrust of research has been focused on the role of repulsive Coulomb interactions between conduction electrons, which naturally explain this pairing symmetry[1]. However, as even simple models based on repulsive interactions have thus far defied a full solution, the question of whether such interactions alone can generate high-temperature superconductivity is still open. A complementary, more empirical approach has asked whether antiferromagnetic spin fluctuations, which are a generic consequence of Coulomb interactions, can mediate Cooper pairing in analogy to the phonon-mediated pairing mechanism in conventional superconductors[2]. This scenario requires the existence of well-defined antiferromagnetic spin fluctuations in the superconducting range of the cuprate phase diagram (for mobile hole concentrations $5\% \leq p \leq 25\%$ per copper atom), well outside the narrow stability range of antiferromagnetic long-range order ($0 \leq p \leq 2\%$).

An extensive series of experiments using inelastic spin-flip scattering of neutrons has indeed revealed low-energy spin fluctuations in doped cuprates[3]. Signatures of coupling between spin and charge excitations have also been identified[4], and evidence has been reported that this coupling is strong enough to mediate superconductivity in underdoped cuprates[5]. However, for cuprate compounds hosting the most robust superconducting states, namely those that are optimally doped to exhibit a superconducting transition temperature $T_c \geq 90$ K, inelastic neutron scattering (INS) experiments have thus far mostly revealed spin excitations over a narrow range of excitation energies $E \sim 30$–70 meV, wave vectors $\mathbf{Q}$ covering only $\sim 10\%$ of the Brillouin-zone area around the

antiferromagnetic ordering wave vector $\mathbf{Q}_{AF}$ and temperatures $T < T_c$ (refs 6–12). The energy- and momentum-integrated intensity of these excitations constitutes only a few per cent of the spectral weight of spin waves in antiferromagnetically ordered cuprates[4,13], and is thus clearly insufficient to support high-T_c superconductivity. Although the recent discovery of a weakly dispersive magnetic excitation in the model system $HgBa_2CuO_{4+\delta}$ with $E \sim 50$ meV may account for some of the missing spectral weight[14], the apparent weakness of antiferromagnetic fluctuations in optimally doped compounds has been used as a central argument against magnetically mediated pairing scenarios for the cuprates[15].

This picture is, however, strongly influenced by technical limitations of the INS method that arise from the small cross-section of magnetic neutron scattering in combination with the weak primary flux of currently available high-energy neutron beams. Because of intensity constraints, even the detection of undamped spin waves in antiferromagnetically ordered cuprates over their full bandwidth of ~ 300 meV has required single-crystal samples with volumes of order 10 cm^3, which are very difficult to obtain[16–19]. Doping further reduces the intensity of the INS profiles and exacerbates these difficulties.

Here we take advantage of recent progress in the development of high-resolution resonant inelastic X-ray scattering (RIXS; see ref. 20 for a review) to explore the doping dependence of magnetic excitations in the widely studied $YBa_2Cu_3O_{6+x}$ family, in a wide energy–momentum window that has been largely hidden from view by INS. As a major result, we demonstrate the existence of spin-wave-like dispersive magnetic excitations (paramagnons) deep inside the electron–hole spin-flip continuum (up to ~ 300 meV), for all the investigated doping levels, with spectral weights comparable to those of magnons in the undoped parent compounds. Exact-diagonalization calculations

1
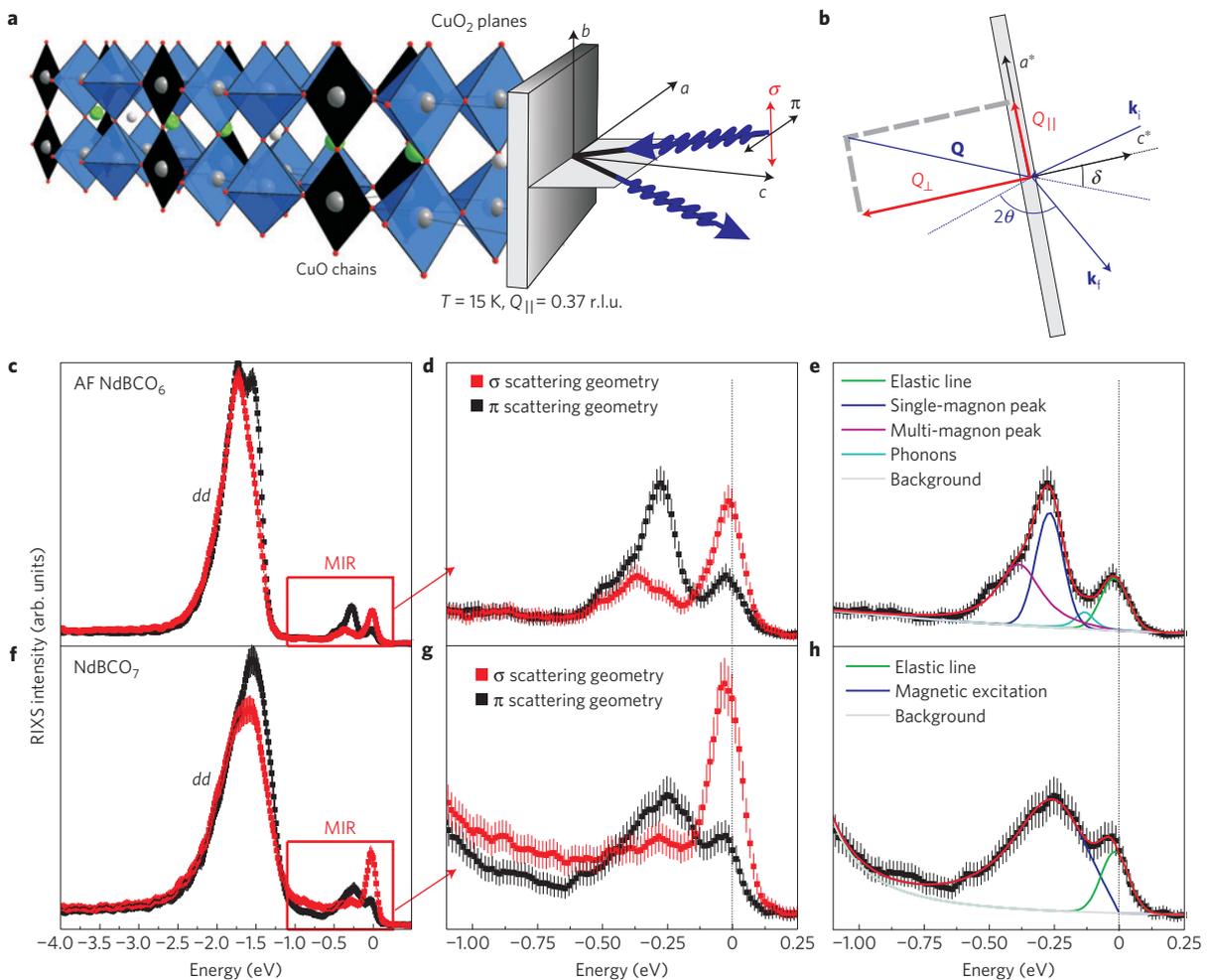
Figure 1 | Scattering geometry and typical Cu L_3-edge RIXS response of cuprates. a,b, Schematic representations of the scattering geometry. **c–h**, Typical RIXS spectra of undoped antiferromagnetic (AF) Nd$_{1.2}$Ba$_{1.8}$Cu$_3$O$_6$ (**c–e**) and superconducting underdoped Nd$_{1.2}$Ba$_{1.8}$Cu$_3$O$_7$ (**f–h**), obtained at $T = 15$ K for $Q_\parallel = 0.37$ r.l.u., in both π (black squares) and σ (red squares) scattering geometries. The error bars indicate the statistical error (s.d. to the number of deteted photons).

of finite-sized hole-doped clusters and an analytical solution of the Eliashberg equations on the basis of the experimentally determined spin excitation spectrum of YBa$_2$Cu$_3$O$_7$ then enable us to quantitatively assess the implications of these observations for the microscopic origin of high-temperature superconductivity.

Experiments on undoped cuprates have shown that RIXS with photon energies at the Cu L_3 absorption edge is sensitive to single-magnon excitations[21–24] by virtue of the strong spin–orbit coupling of the $2p_{3/2}$ core–hole intermediate state[25,26], in excellent agreement with INS measurements[19,27]. Initial RIXS experiments on doped La$_{2-x}$Sr$_x$CuO$_4$ have revealed a complex two-component lineshape with excitations extending up to about 350 meV; the presence of two branches was attributed to phase separation between the superconducting state and a competing state with incommensurate spin and charge order[27]. We have applied the same method to YBa$_2$Cu$_3$O$_{6+x}$ (YBCO$_{6+x}$), Nd$_{1.2}$Ba$_{1.8}$Cu$_3$O$_{6+x}$ (NdBCO$_{6+x}$) and YBa$_2$Cu$_4$O$_8$, which are much less affected by doping-induced disorder and do not show phase separation[28].

Although it is not possible to reach Q_{AF} in cuprates with RIXS at the Cu L_3 edge, one of its great advantages over INS is that it enables measurements of magnetic excitations with sizable intensity over much of the accessible reciprocal space, even on very small sample volumes. The results presented here have been obtained on thin films and on millimetre-sized single crystals far below the volume requirements of INS (see Supplementary Information). Figure 1

shows a sketch of the scattering geometry of our experiment, as well as RIXS spectra obtained on undoped antiferromagnetic NdBCO$_6$ (Fig. 1c,d) and underdoped superconducting NdBCO$_7$ (Fig. 1f,g), for incident photon polarizations in and out of the scattering plane (π and σ geometries) and momentum transfer $Q_\parallel$ along the reciprocal-space a^* direction corresponding to 0.37 reciprocal lattice units (r.l.u.). For both scattering geometries, the spectra exhibit an intense peak located around 1.7 eV energy loss that arises from optically forbidden dd excitations (that is, transitions of the unpaired hole of Cu^{2+} from the $d_{x^2-y^2}$ to other d orbitals)[29] on top of a continuum of charge-transfer excitations. At lower energies, we can see in both compounds an inelastic feature centred around 250 meV and a resolution-limited elastic peak.

For undoped antiferromagnetic NdBCO$_6$, we can decompose the response in the mid-infrared (MIR) region of the spectra (Fig. 1e) for energy losses below ∼500 meV following the method employed in ref. 27. In the π scattering geometry, this leads to (1) an intense resolution-limited peak around 250 meV, (2) a high-energy tail of this peak centred around 400 meV and (3) a weak low-energy contribution around 100 meV. In the σ scattering geometry, feature (1) is strongly suppressed. This polarization dependence enables us to assign this feature to a single-magnon excitation, in agreement with theoretical considerations[24,25] and previous investigations on other cuprates[22–24,27]. This assignment is further confirmed by the disappearance of the MIR inelastic response as the incident photon
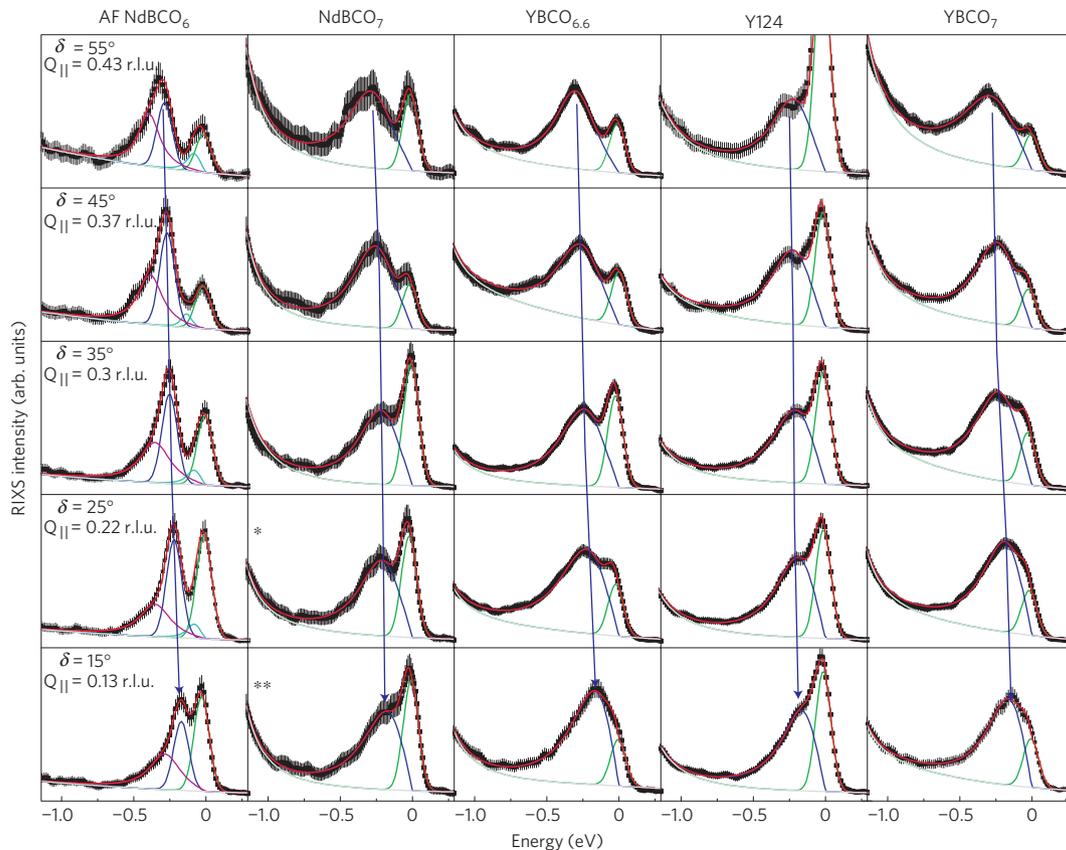
Figure 2 | Experimental data. RIXS response of undoped antiferromagnetic (AF) $Nd_{1.2}Ba_{1.8}Cu_3O_6$ (NdBCO$_6$), underdoped $Nd_{1.2}Ba_{1.8}Cu_3O_7$ (NdBCO$_7$), $YBa_2Cu_3O_{6.6}$ (YBCO$_{6.6}$), $YBa_2Cu_4O_8$ and slightly overdoped $YBa_2Cu_3O_7$ (YBCO$_7$) for various momentum transfers (see Fig. 1), at $T = 15$ K. Note that the spectra for NdBCO$_7$ labelled with an asterisk (two asterisks) were recorded for $\delta = 30°$ ($\delta = 20°$), corresponding to $Q_{\parallel} = 0.26$ (0.18) r.l.u. The error bars indicate the statistical error, and details of the fitting procedure can be found in Supplementary Information.

energy is moved away from the Cu L_3 absorption edge (not shown). The weak features (2) and (3) are associated with higher-order spin excitations and lattice vibrations (single- and multiple-phonon excitations that are not individually resolved), respectively.

The energy of the single-magnon feature in NdBCO$_6$ depends strongly on $Q_{\parallel}$ (left panel of Fig. 2). As the lineshape of the MIR spectrum is $Q_{\parallel}$ independent, the fitting procedure described above can be used to obtain the magnon dispersion relation (see also Supplementary Information). The result shown in Fig. 3a is clearly different from the sinusoidal magnon dispersion observed in La_2CuO_4 (refs 19,27). Indeed, owing to the presence of two antiferromagnetically coupled CuO$_2$ layers per unit cell, two magnon branches with different spin precession patterns are expected[16–18] for NdBCO$_6$: an acoustic branch with intensity $\propto \sin^2(dQ_{\perp}/2)$, where $Q_{\perp}$ is the momentum transfer perpendicular to the CuO$_2$ layers and d is the spacing between the two CuO$_2$ layers, and an optical branch with intensity $\propto \cos^2(dQ_{\perp}/2)$. The result of the calculation of the relative intensities of these two branches for our scattering geometry is shown in the inset of Fig. 3a. It shows that close to the Brillouin zone centre the gapped optical branch dominates. Fitting the momentum dependence of the single-magnon energy of NdBCO$_6$ shown in Fig. 3a using the spin-wave dispersion calculated for a bilayer in the framework of a simple Heisenberg model[16–18], we obtain $J_{\parallel} = 133 \pm 2$ meV and $J_{\perp} = 12 \pm 3$ meV for the intra- and inter-layer exchange constants, respectively, in excellent agreement with the values obtained in antiferromagnetic YBCO$_{6+x}$ (refs 17,18).

We now turn to the doped systems. Figure 2 provides a synopsis of the experimental spectra for all systems investigated here, which span a wide range of doping levels: undoped NdBCO$_6$, strongly underdoped NdBCO$_7$ and YBCO$_{6.6}$ ($T_c = 65$ K and

61 K, respectively), weakly underdoped $YBa_2Cu_4O_8$ ($T_c = 80$ K) and weakly overdoped YBCO$_7$ ($T_c = 90$ K). Because of their stoichiometric composition and electronic homogeneity, the latter two compounds have served as model compounds in the experimental literature on high-T_c superconductivity, but apart from the 'resonant mode' that appears in YBCO$_7$ below T_c (ref. 6) no information has been available on their magnetic excitation spectra. Figure 2 shows that broad MIR features are present at all doping levels in the same energy range as the single-magnon peak in undoped NdBCO$_6$. As these features obey the same polarization dependence as the magnon mode (Fig. 1f,h), they can be assigned to magnetic excitations.

On the basis of the metallic nature of the doped cuprates, we expect strong damping of magnetic excitations in the Stoner continuum of incoherent electron–hole excitations. We have therefore fitted these spectra to Voigt profiles that are the result of the convolution of the Lorentzian lineshape of excitations with finite lifetime with the Gaussian resolution function. This simple fitting procedure yields excellent results (solid lines in Figs 1 and 2) and enables us to extract the energies and half-widths at half-maximum (HWHMs) of the magnetic excitation as a function of the transferred momentum (Fig. 3b,c). In the doped samples, the broadening of the paramagnon profiles due to scattering from charge excitations obliterates the separation between single- and multiple-magnon contributions that is apparent in the undoped case (see Supplementary Information for details).

The magnetic excitation energies of NdBCO$_7$, YBCO$_{6.6}$ and YBCO$_7$ at the Brillouin-zone boundary are nearly identical to the ones found in NdBCO$_6$. This implies that the in-plane exchange constant $J_{\parallel}$ is approximately doping independent, obviating
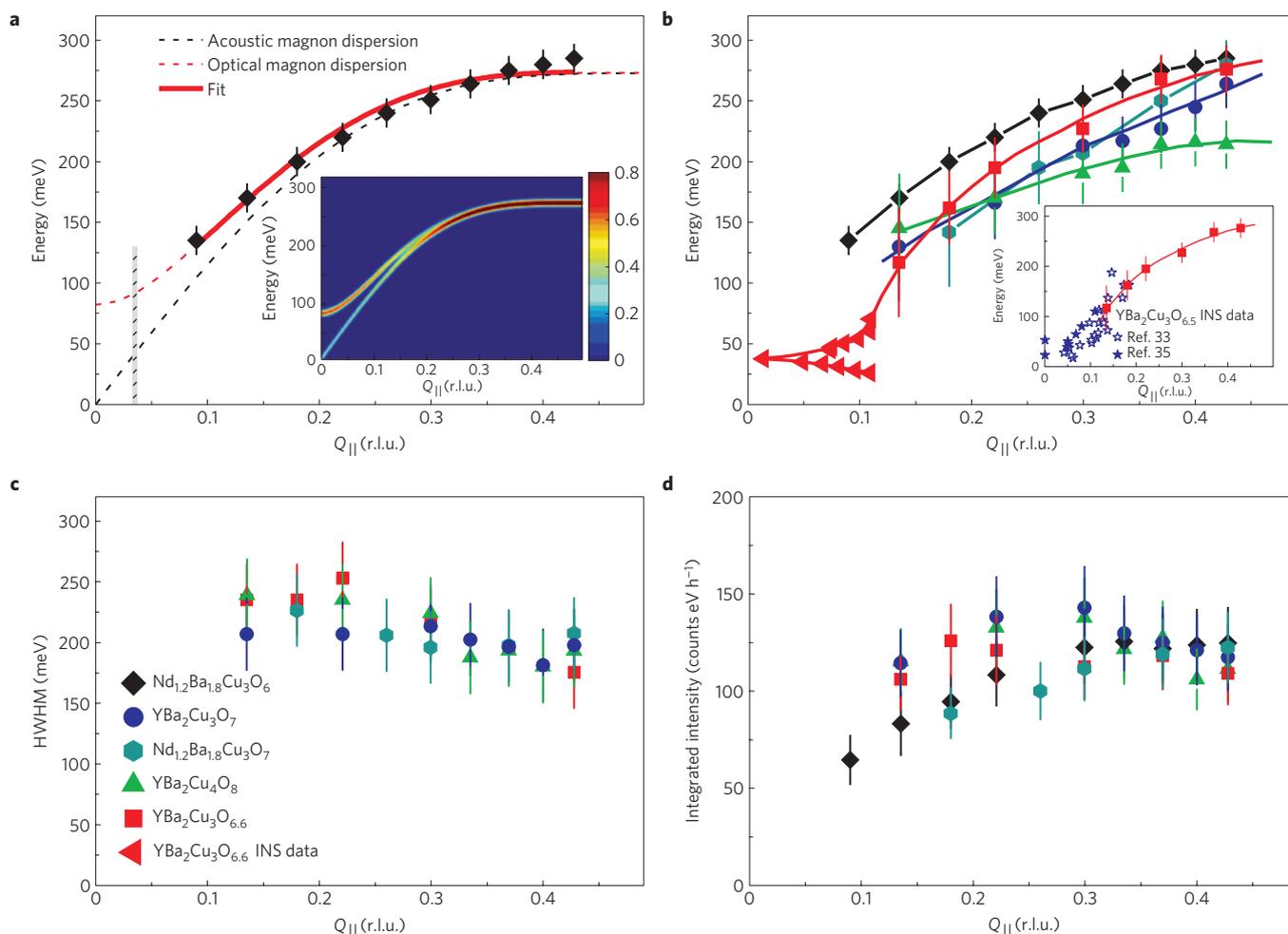
Figure 3 | Dispersion, linewidth and intensity of the magnetic excitations. a, Experimental magnon dispersion along the 100 direction in antiferromagnetic $Nd_{1.2}Ba_{1.8}Cu_3O_6$ at $T = 15$ K, fitted using the spin-wave dispersion of a bilayer from ref. 16 (thick red line). The dashed lines are the acoustic (black) and optical (red) spin-wave dispersions calculated using the fitting parameters. The grey area represents our energy–momentum resolution. Inset: relative intensities of the acoustic and optical magnons for our scattering geometry. **b**, Experimental magnon dispersion along the 100 direction in antiferromagnetic $Nd_{1.2}Ba_{1.8}Cu_3O_6$, underdoped $Nd_{1.2}Ba_{1.8}Cu_3O_7$, $YBa_2Cu_3O_{6.6}$, $YBa_2Cu_4O_8$ and $YBa_2Cu_3O_7$ at $T = 15$ K. Low-frequency INS data recorded along the 100 direction from Q_{AF} for $YBa_2Cu_3O_{6.6}$ have been added[34]. Lines are guides to the eye. **c**, HWHM of magnetic excitations in $Nd_{1.2}Ba_{1.8}Cu_3O_7$, $YBa_2Cu_3O_{6.6}$, $YBa_2Cu_4O_8$ and $YBa_2Cu_3O_7$. **d**, Integrated inelastic intensities. The error bars reflect the accuracy of the fitting procedure detailed in Supplementary Information.

uncertainties associated with previous attempts to extract $J_\parallel$ by extrapolating lower-energy INS data on doped cuprates[30–33]. On approaching the Γ point ($Q_\parallel = 0$), we observe that the dispersion is steeper in the doped compounds than in NdBCO$_6$. Despite the fact that Γ and Q_{AF} are no longer equivalent in the absence of magnetic long-range order, the RIXS data obtained on YBCO$_{6.6}$ nicely extrapolate to the low-energy 'hour-glass' dispersion around Q_{AF} previously extracted from INS data on samples prepared in an identical manner (Fig. 3b; ref. 34). The RIXS data on YBCO$_{6.6}$ are also consistent with recent high-energy INS data on YBCO$_{6.5}$ (ref. 33,35). The combined RIXS–INS data set on YBCO$_{6.6}$ indicates the presence of an inflexion point in the dispersion of the magnetic excitations. We note that the situation seems somewhat different for $YBa_2Cu_4O_8$, where the energy of the magnetic excitations close to the zone boundary is significantly reduced compared with the other systems ($\sim$210 meV instead of $\sim$300 meV), and the dispersion is flatter than in NdBCO$_6$. This may reflect different values of $J_\parallel$ and $J_\perp$ in this system, and deserves further investigation.

The intrinsic HWHM of $\sim$200 meV of the inelastic signal extracted from our data (Fig. 3c) is much larger than the instrumental resolution and comparable to the magnon energies, indicating

strong damping by Stoner excitations. The damping rate does not change substantially with $Q_\parallel$ or with doping. Finally, whereas it is not yet possible to obtain absolute magnetic intensities from RIXS data, we can extract the relative intensity of the RIXS profiles by integrating the inelastic signal in the MIR region (see Supplementary Information). Remarkably, the integrated intensity obtained in this way is conserved on doping from the antiferromagnetic insulator to the slightly overdoped superconductor.

We have thus demonstrated the existence of paramagnons, that is, damped but well-defined dispersive magnetic excitations, deep in the Stoner continuum of cuprates with doping levels beyond optimal doping. Their spectral weights are similar to those of spin waves in the undoped, antiferromagnetically ordered parent material. These excitations have thus far not been observed by INS due to the much less favourable counting rates and signal-to-background ratios in INS experiments on doped cuprates[3,6–12,30–34].

To obtain insight into the origin of this surprising observation, we have carried out exact-diagonalization calculations of the t–J Hamiltonian with the exchange coupling constant $J = 0.3t$ (t is the nearest-neighbour hopping) on finite-sized clusters, following the method proposed in refs 36–38. We used clusters with 18 and 20
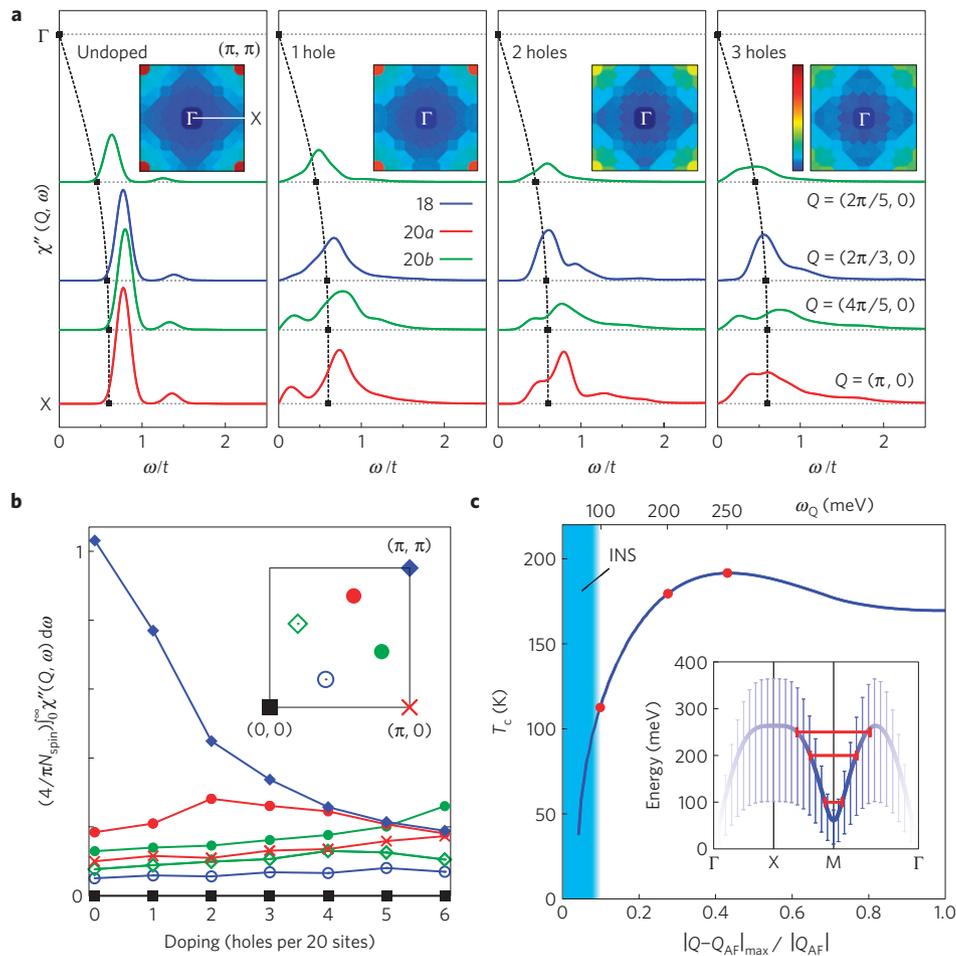
Figure 4 | Results of model calculations. a, Imaginary part of the spin susceptibility $\chi''(Q,\omega)$ resulting from exact diagonalization of the t–J model with $J/t = 0.3$ on small clusters. Results from 18-site and two 20-site clusters are combined to cover the Γ–X line (see Supplementary Information). The spectra are broadened using a Gaussian with HWHM $= 0.1t$. Dashed lines correspond to the linear spin-wave dispersion with the same J as used in numerics. Insets: Brillouin-zone maps of energy-integrated χ'' with a common colour scale. **b**, Energy-integrated χ'' of the 20-site cluster, normalized to the number of electrons on the cluster, as a function of doping. The seven accessible non-equivalent $\mathbf{Q}$ vectors for this cluster are shown in the inset. **c**, Superconducting transition temperature resulting from the Eliashberg calculation for the experimentally determined spin excitation spectrum of YBCO$_7$ shown in the inset. Vertical bars account for the experimentally determined linewidth of the excitations. The red lines indicate the influence of successive momentum-space cutoffs limiting the maximum distance from $\mathbf{Q}_{\text{AF}}$ of the $\mathbf{Q}$ vectors for which $\chi(\mathbf{Q},\omega)$ is included in the calculation.

spins arranged in various shapes to map the $(H,K,0)$ reciprocal plane with sufficient momentum resolution (see Supplementary Information). The resulting spectra were convoluted by a Gaussian function with HWHM $0.1t$ to simulate the experimental resolution function. The calculated imaginary part of the spin susceptibility is shown in Fig. 4a for different hole concentrations. In the undoped case, we can observe two peaks in the imaginary part of the spin susceptibility: an intense peak corresponding to the single-magnon excitation, and a weaker feature at higher energy corresponding to higher-order processes. The single-magnon peak clearly disperses, although its energy is slightly above the value expected from linear spin-wave theory (dotted lines), due to the finite size of the cluster. In the inset of Fig. 4a, we present the energy-integrated magnetic intensity in the $(H,K,0)$ reciprocal plane. As expected, the intensity in the undoped situation is strongly peaked at $\mathbf{Q}_{\text{AF}}$, and fairly uniformly distributed in the rest of the plane. As holes are added to the clusters, the magnetic spectral weight strongly decreases only around $\mathbf{Q}_{\text{AF}}$, and remains essentially constant everywhere else. This can also be seen in Fig. 4b, where the imaginary part of the energy-integrated spin susceptibility is plotted as a function of doping. The experimental and numerical data are thus in excellent agreement.

Armed with essentially complete knowledge of the spin-fluctuation spectrum, and motivated by the agreement with the numerical data for the t–J model, we now estimate the superconducting transition temperature T_c generated by a Cooper-pairing mechanism in which the experimentally detected spin fluctuations play the role of bosonic glue. To this end, we have self-consistently solved the Eliashberg equations using the vertex function of the t–J model[39] and the experimental spin-fluctuation spectrum of YBCO$_7$ (Fig. 4c inset), without adjustable parameters. Details are given in Supplementary Information. Figure 4c shows the outcome of the calculation. The resulting T_c of 170 K is similar to the maximum T_c observed in the cuprates and to another recent estimate based on the comparison of INS and photoemission data on underdoped YBCO$_{6+x}$ (ref. 5). The agreement with the experimentally observed T_c of YBCO$_7$ is satisfactory in view of ignoring vertex corrections beyond Eliashberg theory and other simplifying assumptions in the calculation, and in view of a similar level of quantitative agreement reported for Eliashberg calculations of conventional low-T_c superconductors[40]. To resolve the relative contribution of the strongly doping-dependent region around $\mathbf{Q}_{\text{AF}}$ and the high-energy part of the spin susceptibility revealed by RIXS to the

pairing strength, we have introduced momentum cutoffs around $\mathbf{Q}_{AF}$ in the calculation (Fig. 4c). Clearly, both low- and high-energy spin fluctuations contribute substantially to the pairing. In underdoped cuprates with lower gaps and stronger antiferromagnetic correlations, vertex corrections are expected to become essential[41], reducing the T_c values calculated here. These corrections suppress coupling to magnons in the vicinity of $\mathbf{Q}_{AF}$, leaving the contribution of the higher-energy excitations as a vital source of pairing.

References

1. Scalapino, D. J. The case for $d_{x^2-y^2}$ pairing in the cuprate superconductors. *Phys. Rep.* **250,** 329–365 (1995).
2. Abanov, A., Chubukov, A. V. & Schmalian, J. Quantum-critical theory of the spin fermion model and its application to cuprates: Normal state analysis. *Adv. Phys.* **52,** 119–218 (2003).
3. Birgeneau, R. J., Stock, C., Tranquada, J. M. & Yamada, K. Magnetic neutron scattering in hole-doped cuprate superconductors. *J. Phys. Soc. Jpn* **75,** 111003 (2006).
4. Eschrig, M. The effect of collective spin-1 excitations on electronic spectra in high-T_c superconductors. *Adv. Phys.* **55,** 47–183 (2006).
5. Dahm, T. *et al.* Strength of the spin-fluctuation-mediated pairing interaction in a high-temperature superconductor. *Nature Phys.* **5,** 217–221 (2009).
6. Fong, H. F. *et al.* Polarized and unpolarized neutron-scattering study of the dynamical spin susceptibility of YBa$_2$Cu$_3$O$_7$. *Phys. Rev. B* **54,** 6708–6720 (1996).
7. Hayden, S. M. *et al.* The structure of the high-energy spin excitations in a high-transition-temperature superconductor. *Nature* **429,** 531–534 (2004).
8. Hinkov, V. *et al.* Two-dimensional geometry of spin excitations in the high-transition-temperature superconductor YBa$_2$Cu$_3$O$_{6+x}$. *Nature* **430,** 650–653 (2004).
9. He, H. *et al.* Magnetic resonant mode in the single-layer high-temperature superconductor Tl$_2$Ba$_2$CuO$_{6+\delta}$. *Science* **295,** 1045–1047 (2002).
10. Reznik, D. *et al.* Local-moment fluctuations in the optimally doped high-T_c superconductor YBa$_2$Cu$_3$O$_{6.95}$. *Phys. Rev. B* **78,** 132503 (2008).
11. Xu, G. *et al.* Testing the itinerancy of spin dynamics in superconducting Bi$_2$Sr$_2$CaCu$_2$O$_{8+\delta}$. *Nature Phys.* **5,** 642–646 (2009).
12. Yu, G. *et al.* Magnetic resonance in the model high-temperature superconductor HgBa$_2$CuO$_{4+\delta}$. *Phys. Rev. B* **81,** 064518 (2010).
13. Kee, H-Y., Kivelson, S. A. & Aeppli, G. Spin-1 neutron resonance peak cannot account for electronic anomalies in the cuprate superconductors. *Phys. Rev. Lett.* **88,** 257002 (2002).
14. Li, Y. *et al.* Hidden magnetic excitation in the pseudogap phase of a high-T_c superconductor. *Nature* **468,** 283–285 (2010).
15. Maksimov, E. G., Kuli'c, M. L. & Dolgov, O. V. Bosonic spectral function and the electron–phonon interaction in HTSC cuprates. *Adv. Cond. Mat. Phys.* **2010,** 423725 (2010).
16. Tranquada, J. M. *et al.* Neutron scattering study of magnetic excitations in YBa$_2$Cu$_3$O$_{6+x}$. *Phys. Rev. B* **40,** 4503–4516 (1989).
17. Reznik, D. *et al.* Direct observation of optical magnons in YBa$_2$Cu$_3$O$_{6.2}$. *Phys. Rev. B* **53,** R14741–R14744 (1996).
18. Hayden, S. M. *et al.* High-frequency spin waves in YBa$_2$Cu$_3$O$_{6.15}$. *Phys. Rev. B* **54,** R6905–R6908 (1996).
19. Coldea, R. *et al.* Spin waves and electronic interactions in La$_2$CuO$_4$. *Phys. Rev. Lett.* **86,** 5377–5380 (2001).
20. Ament, L. J. P. *et al.* Resonant inelastic X-ray scattering studies of elementary excitations. *Rev. Mod. Phys.* **83,** 705–767 (2011).
21. Braicovich, L. *et al.* Dispersion of magnetic excitations in the cuprate La$_2$CuO$_4$ and CaCuO$_2$ compounds measured using resonant X-ray scattering. *Phys. Rev. Lett.* **102,** 167401 (2009).
22. Schlappa, J. *et al.* Collective magnetic excitations in the spin ladder Sr$_{14}$Cu$_{24}$O$_{41}$ measured using high-resolution resonant inelastic X-ray scattering. *Phys. Rev. Lett.* **103,** 047401 (2009).
23. Guarise, M. *et al.* measurement of magnetic excitations in the two-dimensional antiferromagnetic Sr$_2$CuO$_2$Cl$_2$ insulator using resonant X-ray scattering: Evidence for extended interactions. *Phys. Rev. Lett.* **105,** 157006 (2010).
24. Braicovich, L. *et al.* Momentum and polarization dependence of single-magnon spectral weight for Cu L_3-edge resonant inelastic X-ray scattering from layered cuprates. *Phys. Rev. B* **81,** 174533 (2010).
25. Ament, L. J. P. *et al.* Theoretical demonstration of how the dispersion of magnetic excitations in cuprate compounds can be determined using resonant inelastic X-ray scattering. *Phys. Rev. Lett.* **103,** 117003 (2009).
26. Haverkort, M. W. Theory of resonant inelastic X-ray scattering by collective magnetic excitations. *Phys. Rev. Lett.* **105,** 167404 (2010).
27. Braicovich, L. *et al.* Magnetic excitations and phase separation in the underdoped La$_{2-x}$Sr$_x$CuO$_4$ superconductor measured by resonant inelastic X-ray scattering. *Phys. Rev. Lett.* **104,** 077002 (2010).
28. Bobroff, J. *et al.* Absence of static phase separation in the high T_c cuprate YBa$_2$Cu$_3$O$_{6+y}$. *Phys. Rev. Lett.* **89,** 157002 (2002).
29. Ghiringhelli, G. *et al.* Low energy electronic excitations in the layered cuprates studied by copper L_3 resonant inelastic X-ray scattering. *Phys. Rev. Lett.* **92,** 117406 (2004).
30. Stock, C. *et al.* From incommensurate to dispersive spin-fluctuations: The high-energy inelastic spectrum in superconducting YBa$_2$Cu$_3$O$_{6.5}$. *Phys. Rev. B* **71,** 024522 (2005).
31. Vignolle, B. *et al.* Two energy scales in the spin excitations of the high-temperature superconductor La$_{2-x}$Sr$_x$CuO$_4$. *Nature Phys.* **3,** 163–167 (2007).
32. Lipscombe, O. J. *et al.* Emergence of coherent magnetic excitations in the high temperature underdoped La$_{2-x}$Sr$_x$CuO$_4$ superconductor at low temperatures. *Phys. Rev. Lett.* **102,** 167002 (2009).
33. Stock, C. *et al.* Effect of the pseudogap on suppressing high energy inelastic neutron scattering in superconducting YBa$_2$Cu$_3$O$_{6.5}$. *Phys. Rev. B* **82,** 174505 (2010).
34. Hinkov, V. *et al.* Spin dynamics in the pseudogap state of a high-temperature superconductor. *Nature Phys.* **3,** 780–785 (2007).
35. Bourges, P. *et al.* High-energy spin excitations in YBa$_2$Cu$_3$O$_{6.5}$. *Phys. Rev. B* **56,** R11439 (1997).
36. Tohyama, T., Horsch, P. & Maekawa, S. Spin and charge dynamics of the t–J model. *Phys. Rev. Lett.* **74,** 980–983 (1995).
37. Eder, R., Ohta, Y. & Maekawa, S. Anomalous spin and charge dynamics of the t–J model at low doping. *Phys. Rev. Lett.* **74,** 5124–5127 (1995).
38. Dagotto, E. Correlated electrons in high-temperature superconductors. *Rev. Mod. Phys.* **66,** 763–840 (1994).
39. Prelovšek, P. & Ramšak, A. Spectral functions and the pseudogap in the t–J model. *Phys. Rev. B* **63,** 180506(R) (2001).
40. Carbotte, J. P. Properties of boson-exchange superconductors. *Rev. Mod. Phys.* **62,** 1027–1157 (1990).
41. Schrieffer, J. R. Ward's identity and the suppression of spin fluctuation superconductivity. *J. Low Temp. Phys.* **99,** 397–402 (1995).

Author contributions

M.L.T., G.G., L.B., V.H. and B.K. managed the project. Y.T.S., G.L.S. and C.T.L. grew the single-crystalline samples; G.M.D.L. and M.S. prepared the thin films. M.L.T., G.G., M.M.S., V.H., M.M., M.B., S-B.C. and L.B. carried out the experiment assisted by K.J.Z., C.M. and T.S. M.L.T. and L.B. analysed the data. J.C., G.K. and M.W.H. carried out the theoretical calculations. M.L.T. and B.K. wrote the paper with comments from all co-authors.

Additional information

The authors declare no competing financial interests. Supplementary information accompanies this paper on www.nature.com/naturephysics. Reprints and permissions information is available online at http://www.nature.com/reprints. Correspondence and requests for materials should be addressed to M.L.T. or B.K.